UC Santa Barbara

UC Santa Barbara Previously Published Works

Authors

Jin, Hongjun

Zhang, Xiang

Yue, Xuyi

et al.

Kinetics Modeling and Occupancy Studies of a Novel C-11 PET Tracer for VAChT in Nonhuman Primates

Hongjun Jin[1], **Xiang Zhang**[1], **Xuyi Yue**[1], **Hui Liu**[1], **Junfeng Li**[1], **Hao Yang**[1], **Hubert Flores**[2], **Yi Su**[2], **Stanley M. Parsons**[3], **Joel S. Perlmutter**[1,2], and **Zhude Tu**[1,*]

[1]Department of Radiology, Washington University School of Medicine, St. Louis, MO 63110, USA

[2]Department of Neurology, Washington University School of Medicine, St. Louis, MO 63110, USA

[3]Department of Chemistry and Biochemistry, University of California, Santa Barbara, CA 93106, USA

Abstract

Introduction—Deficits in cholinergic function have been found in the aged brain and in neurodegenerative diseases including Alzheimer's disease (AD) and Parkinson's disease (PD). The vesicular acetylcholine transporter (VAChT) is a reliable biomarker for the cholinergic system. We previously reported the initial *in vitro* and *ex vivo* characterization of (–)-[^{11}C]**TZ659** as a VAChT specific ligand. Here, we report the *in vivo* specificity, tracer kinetics, and dose-occupancy studies in the nonhuman primate brain are reported.

Methods—MicroPET brain imaging of (–)-[^{11}C]**TZ659** was performed under baseline conditions in two male macaques. Tracer kinetic modeling was carried out using a two-tissue compartment model (2TCM) and Logan plot with arterial blood input function and using a simplified reference tissue model (SRTM) and Logan plot (LoganREF) without blood input. Specificity for VAChT was demonstrated by pretreatment with (+)-pentazocine, (–)-vesamicol, or *S*-(–)-eticlopride. Target occupancy (Occ) was calculated following pretreatment with escalating doses of (–)-vesamicol.

Results—Baseline PET imaging revealed selective retention in the striatum with rapid clearance from the cerebellar hemispheres as a reference region. Total volume of distribution (V_T) values derived from both 2TCM and Logan analysis with blood input revealed ~3-fold higher levels of (–)-[^{11}C]TZ659 in the striatum than the cerebellar hemispheres. Injection of (–)-vesamicol either as a blocking or displacing agent significantly reduced striatal uptake of (–)-[^{11}C]**TZ659**. In contrast, pretreatment with the sigma-1 ligand (+)-pentazocine had no impact. Pretreatment with the *S*-(–)-eticlopride, a dopamine D_2–like receptor antagonist, increased striatal uptake of (–)-[^{11}C]**TZ659**. Striatal binding potential (BP_{ND}, range of 0.33 – 1.6 with cerebellar hemispheres as the reference region) showed good correlation ($r^2 = 0.97$) between SRTM and LoganREF.

Occupancy studies found that ~ 0.0057 mg/kg (−)-vesamicol produced 50% VAChT occupancy in the striatum.

Conclusion—(−)-[11C]**TZ659** demonstrated specific and reversible VAChT binding and favorable pharmacokinetic properties for assessing the density of VAChT in the living brain.

Keywords

tracer kinetics; vesicular acetylcholine transporter; (−)-[11C]**TZ659**; binding potential; occupancy

1. Introduction

The cholinergic hypothesis states that functional disturbances in cholinergic activity in the brain of aged subjects and patients with dementia play an important role in memory loss and related cognitive problems. Thus, restoration of cholinergic function may reduce the severity of the cognitive loss [1, 2]. Although pathological and pharmacological studies have provided considerable supporting evidence [3], the cholinergic hypothesis has been challenged by post-mortem findings that suggest that choline acetyltransferase (ChAT) and acetylcholinesterase (AChE) are not reduced in neocortical tissues of patients with mild AD [4, 5]. These findings may not accurately reflect *in vivo* cholinergic function considering the stability of these enzymes. Noninvasive *in vivo* imaging techniques are urgently needed to study changes in cholinergic function in patients with cognitive dysfunction [6, 7]. PET imaging with a suitable radiotracer could provide a highly sensitive non-invasive imaging modality that is able to directly quantify cholinergic deficits in living subjects. As a primary signaling molecule for cholinergic neurons, newly synthesized ACh is transported into synaptic vesicles by the vesicular acetylcholine transporter (VAChT) which is a very slow transporter [8–12]. VAChT acts as a limiting factor for release of the neurotransmitter (ACh) and plays a critical role in the cholinergic system [2]. VAChT is considered to be a reliable marker for cholinergic function and a suitable target for molecular imaging with PET [13, 14]. (−)-Vesamicol binds in a stereoselective, non-competitive manner to VAChT [15, 16]. It acts as an allosteric antagonist of ACh uptake by presynaptic vesicles, thus inhibiting storage and release of ACh in the cholinergic nerve terminal. Although the pharmacology of (−)-vesamicol and the localization of its binding site to cholinergic terminals were described in the 1980's, the high affinity of (−)-vesamicol for the sigma-1 receptor in the central nervous system (CNS) limited its utility for VAChT imaging. Numerous modified (−)-vesamicol analogues have been reported as potent and selective VAChT inhibitors [17–23]. Although many promising ligands proceeded to subsequent radiolabeling for preliminary evaluation in rodents, only a limited number of them have been evaluated in nonhuman primate (NHP) or human subjects [18, 19, 21, 24–26]. Recently, the results of radiation dosimetry and the first PET imaging studies of (−)-5-18F-fluoroethoxybenzovesamicol ([18F]-FEOBV) were reported for ten human subjects [24]. Although equilibrium kinetics in the brain of both NHP and human subjects show delayed equilibrium of > 360 min post injection (p.i.), [18F]FEOBV offers advantages over SPECT ligands for cholinergic terminal brain imaging [24].

Our group reported a number of VAChT inhibitors containing a carbonyl group attached to the 4-position of the piperidine ring and reported the structure–activity relationships of these

new compounds [18, 19, 26, 27]. The most promising ligands were radiolabeled, and we had performed preliminary evaluation in rodents and NHPs. Among these, (–)-[11C]**TZ659** demonstrated favorable initial results during *in vivo* evaluation in rats and preliminary CNS imaging studies in a male macaque [27, 28]. Here we further demonstrate *in vivo* binding specificity of (–)-[11C]**TZ659** for VAChT in healthy adult male NHPs under physiological conditions (baseline) and different pharmacological challenge conditions. Our results revealed that (–)-[11C]**TZ659** binds specifically to the VAChT-enriched striatum. The uptake of (–)-[11C]TZ659 was both blocked and displaced using the known VAChT ligand, (–)-vesamicol. Pretreatment with a sigma-1 receptor ligand did not impact striatal uptake of (–)-[11C]**TZ659**, while pretreatment with the dopamine D_2–like receptor antagonist (–)-eticlopride increased striatal uptake of (–)-[11C]**TZ659**. To estimate the dose for 50% occupancy of VAChT in the striatum, a series of PET studies of (–)-[11C]**TZ659** after pretreatment of the same subject using different doses of (–)-vesamicol were performed; these studies demonstrated that (–)-[11C]**TZ659** PET imaging can be used to calculate VAChT occupancy.

2. Materials and methods

2.1. Radiosynthesis

The synthesis of (–)-**TZ659** and the radiolabeling of (–)-[11C]**TZ659** were accomplished as previously described [27]. The radiochemical yield was 40–50% (decay corrected to end of bombardment (EOB)) with a radiochemical purity > 99%, the chemical purity of > 95%, and the specific activity was >74 kBq /μmol (decay corrected to EOB).

2.2. Nonhuman primate microPET studies

2.2.1. Subjects—All animal experiments were conducted in compliance with the Guide for the Care and Use of Research Animals under protocols approved by the Washington University School of Medicine Animal Studies Committee. PET scans of the NHP brain were carried out on two adult male cynomolgus macaques weighing 5.5–7.5 kg following established procedures.[26, 29–31] Subject A underwent four baseline scans (including two scans with two arterial blood sampling) and seven scans following pharmacological intervention. Subject B underwent two baseline scans (including one scan with arterial blood sampling). Known compounds were purchased from Sigma Aldrich; (–)-vesamicol was resolved in-house from racemic vesamicol; all doses were freshly prepared for each study and aseptically filtered for intravenous (i.v.) injection. As described below, binding specificity was evaluated in NHP Subject A following pretreatment with the sigma-1 receptor compound (+)-pentazocine, the dopamine D_2–like receptor antagonist *S*-(–)-eticlopride hydrochloride, and displacement with (–)-vesamicol. Subject A also underwent a series of scans following pretreatment using escalating doses of (–)-vesamicol prior to administration of (–)-[11C]**TZ659**.

2.2.2. PET data acquisition—Imaging studies of (–)-[11C]**TZ659** were carried out on a microPET Focus 220 scanner (Concorde/CTI/Siemens Microsystems, Knoxville, TN). Animals were fasted for 12 h before the PET scan, each animal was initially anesthetized with ketamine (10 mg/kg) and glycopyrrolate (0.013 mg/kg) intramuscularly for

transportation to the PET suite. Upon arrival at the scanner, the subject was intubated and anesthetized with ~2% isoflurane in oxygen. A percutaneous catheter was placed in the femoral vein for injection of tracer or pharmacological agents; an additional percutaneous catheter was placed in the contralateral femoral artery to permit arterial blood sampling as needed. The monkey's head was positioned supine in the head holder with the brain in the center of the field of view. Anesthesia was maintained at 0.75−2.0% during the scan and core temperature was maintained at ~37 °C; vital signs were monitored every 5 min. After a 10 min transmission scan to confirm positioning of the brain within the scanner; a 45 min transmission scan was performed for attenuation correction. After transmission scans, a 120 min dynamic (3×1-min, 4×2-min, 3×3-min, and 20×5-min frames) emission scan was acquired after i.v. injection of 299.7 – 418.1 MBq of (−)-[^{11}C]**TZ659** in 10% ethanol saline solution.

Occupancy of (−)-vesamicol for VAChT was determined by pretreatment of the animal using escalating doses (0.01, 0.05, 0.125, and 0.25 mg/kg) of (−)-vesamicol, a potent allosteric antagonist of VAChT, administered i.v. to NHP Subject A ~6 min prior to injection of (−)-[^{11}C]**TZ659**. Pretreatment using the sigma-1 receptor ligand (+)-pentazocine (1.0 mg/kg, i.v., 12 min prior to tracer injection) was similarly performed to determine specificity for radiotracer binding towards VAChT *versus* the sigma-1 receptor. The dopamine D_2-like receptor antagonist *S*-(−)-eticlopride [32, 33] was used to demonstrate the change in striatal cholinergic activity following treatment with *S*-(−)-eticlopride (0.025 mg/kg) administered i.v. 5 min prior to tracer injection. Displacement studies were conducted in NHP Subject A by treatment with 0.3 mg/kg (−)-vesamicol, administered i.v. 20 min post radiotracer injection.

2.2.3. PET image processing—PET scans from all studies were corrected by using individual attenuation and model-based scatter correction, and reconstructed using filtered back projection as described previously [34]. The reconstructed resolution in the PET image was < 2.0 mm full width half maximum for all 3 dimensions at the center of the field of view. The subject's magnetization-prepared rapid gradient-echo (MP-RAGE) MR image (collected from 3T Trio MRI Scanner), and the summed 30 frames PET images were co-registered using AIR method [35, 36]. For quality control of the co-registration process, the co-registered PET and MRI were superimposed using Vidi or Analyzer program (AnalyzeDirect Inc., Overland Park, KS) and any misalignments could be detected by a misposition of brain edges on both images. For quantitative analyses, three-dimensional regions of interest (ROI) for striatum, frontal cortex, occipital cortex, temporal cortex, white matter, midbrain, hippocampus and cerebellar hemispheres, were identified on the MRI and then transformed into baseline PET space using the co-registration transformation matrix. These ROIs were then used to extract TACs from the dynamic PET images. Radioactivity measurements were standardized to the body weight and the dose of radioactivity injected to yield standardized uptake value (SUV). To minimize noise, the signal in the presentation TAC data have been smoothed by "Adjacent Averaging" using the OriginLab 9.1 program (OriginLab Corporation, Northampton, MA). All imaging analysis and tracer kinetic modeling were based on the original data without smoothing.

2.3. Arterial blood input function for tissue compartment kinetics modeling

To determine the arterial input function curve and radioactive metabolite fraction, arterial blood samples were collected from the femoral artery at different time points after injection of (−)-[11C]**TZ659**. Arterial samples were collected during the first 5 min using an automated blood sampling system with a peristaltic pump that pulls arterial blood at 5 mL/min through a plastic scintillator for radioactivity detection; counts were binned using LabVIEW software (National Instruments Corporation, Austin, TX). Additional arterial samples (2–3 mL) were manually collected in heparinized syringes at 2, 5, 10, 15, 30, 60 and 90 min p.i. for measurement of radiolabeled metabolites. Aliquots of whole blood (1 mL) were counted in a well gamma counter (Brinkmann Instruments Inc, NY), then centrifuged at $2,500 \times g$ in an Eppendorf 5415C centrifuge (Eppendorf North America, Inc.) for 5 min to separate red blood cells from plasma. Portions of plasma (400 μL) were solvent-deproteinated using 0.92 mL ice-cold methanol and separated by centrifugation at $2,500 \times g$. The supernatant was mixed with water (1/1, v/v) and the mixture was injected into a HPLC system for radioactive metabolite determination. The HPLC system consisted of an Agilent SB C-18 analytic HPLC column (250 mm × 4.6 mm, 5 μm) and an UV detector with wavelength set at 254 nm. The mobile phase was acetonitrile/ 0.1 M, pH 4.5 ammonium formate buffer (52/48, v/v), and the flow rate was 1.0 mL/min. The HPLC fractions were collected at 1 min intervals for 16 min; each fraction was counted on a well counter. The counts were corrected for background radiation and physical decay. The sample recovery rate, extraction efficiency, and HPLC fraction recovery were calculated by measuring radioactivity in the plasma HPLC fractions. The parent fraction was determined as the ratio of the radioactivity of the parent (standard) compound to the total amount of radioactivity collected. These time-dependent measures were modeled to permit calculation of a true (−)-[11C]**TZ659** TAC from the total radioactivity measured by the automated blood sampling system. The metabolite corrected arterial blood TAC was fitted with 2TCM model [37] and Logan plot [38, 39] using the TAC from the PET measurements. In 2TCM with metabolite corrected arterial blood input function, the PET data and TAC were fitted by the equation [37] to estimate the K_1, k_2, k_3 and k_4 by nonlinear regression using a MATLAB (Mathworks Inc., Natick, MA). The value of V_T was estimated by $K_1/k_2 *(1+k_3/k_4)$. In the Logan plot graphic analysis, V_T for the given ROI was derived from the slope of the linear plot $\int_0^T C_{ROI} dt / C_{RO_I}$ versus $\int_0^T C_P dt / C_{RO_I}$ with the metabolite-corrected arterial blood input function [38, 39].

2.4. Reference based tracer kinetic analysis

Quantification of specific uptake was also performed with two reference-based tracer kinetic methods: Logan Reference (LoganREF) [38, 39] model and SRTM [39, 40]. The cerebellar hemisphere (excluding cerebellum vermis) was used as a reference region in both models. Using the LoganREF model, the distribution volume ratio (DVR) was estimated in each ROI including striatum, frontal cortex, occipital cortex, temporal cortex, white matter, midbrain and hippocampus using a MATLAB (Mathworks Inc., Natick, MA) implementation of these tracer kinetic methods as previously published [38]. This enabled calculation of the binding potential (non-displaceable): $BP_{ND} = DVR-1$, which is proportional to the ratio B_{max}/K_d for each ROI with a fixed k_2' value 0.1 min^{-1} (average k_2' value was based on 2TCM

modeling with arterial blood input) and C_{ROI} values collected from the PET scans. BP_{ND} and R_1, k_2 values were also derived from the application of SRTM model. The model fitting was processed as previously published [40, 41] with C_R (reference region tracer radioactivity concentration) and C_T (target region tracer radioactivity concentration) values derived from microPET collections. Baseline values for these studies represent the average of the four scans of Subject A and two scans of Subject B.

The regional target occupancy (Occ) following pretreatment using cold (−)-vesamicol was calculated directly as the relative change in striatal BP_{ND} using SRTM; and it refers to the percentage of the target specific VAChT binding sites bound by the drug molecule ((−)-vesamicol):

$$Occ\% = \frac{BP_{ND}^{Baseline} - BP_{ND}^{Drug-treatment}}{BP_{ND}^{Baseline}} \times 100\%$$

The occupancy values were averaged across the striatal regions (putamen and caudate) to estimate the occupancy percentage. In addition, the occupancy values for all regions at baseline and after the animal was pretreated using (−)-vesamicol were analyzed using the LoganREF occupancy plot [42], to provide alternative estimates of the reduction in the specific signal.

3. Results

3.1. NHP baseline imaging and tracer specificity study

PET images of summed radioactivity from 0 to 120 min, showing the regional distribution of (−)-[^{11}C]**TZ659** at baseline, are depicted in Figure 1. Baseline scans showed specific retention in the VAChT enriched striatum, and rapid washout kinetics, with a good contrast to non-target regions. The target to non-target (striatum-to-cerebellar hemispheres) ratio (indicated by SUV) reached 1.5 by 30–40 min post injection, and gradually increased to greater than 2.0 after 60 min as radioactivity washed out of the cerebellum rapidly. Peak striatal steady state for (−)-[^{11}C]**TZ659** was observed ~20 min p.i.

Pretreatment with the allosteric antagonist (−)-vesamicol at a dose of 0.25 mg/kg caused a significant decrease of the striatal uptake. Pretreatment with the sigma-1 receptor compound (+)-pentazocine did not change the striatal uptake (Figure 1). Notably, pretreatment with the dopamine D_2–like receptor antagonist S-(−)-eticlopride resulted in increase of the striatal uptake of (−)-[^{11}C]**TZ659** by about 1.5-fold at steady state, compared with baseline (Figure 1). This is consistent with early published reports of increased striatal uptake of a SPECT imaging agent for VAChT in eticlopride-treated rats [43].

3.2. Tracer kinetics

Three independent arterial blood collections during baseline PET scans were carried on NHP Subject A (n=2) and Subject B (n=1). TACs for reference regions in the brain were analyzed with 2TCM using metabolite-corrected plasma as the input function following the published protocol [37]. In general, the 2TCM model fitted the observed brain TACs well,

permitting good estimates of tracer kinetics values, as summarized in Table 1. The estimated values are reported as mean and standard deviation (mean ± SD) from three independent baseline scans. The K_1 (rate constant for transfer from plasma to brain regions) values for striatum and cerebellar hemisphere were 0.18 ± 0.05 and 0.23 ± 0.05 mL g^{-1} tissue min^{-1} respectively, which are consistent with good blood-brain barrier penetration of (–)-[11C]**TZ659** [27]. The k_2 (rate constant for transfer of tracer from brain regions to plasma) values for striatum and cerebellar hemispheres were 0.052 ± 0.02 and 0.11 ± 0.03 min^{-1} respectively. The higher value of k_2 for cerebellar hemispheres than for striatum indicates a faster washout from the cerebellar hemisphere reference region. The average k_3 (association rate constant for tracer binding to tissue) values for striatum and cerebellar hemispheres were 0.041 ± 0.006 and 0.019 ± 0.001 min^{-1} respectively, indicating the tracer binds to striatum more favorably. The average k_4 (dissociation rate constant) values for striatum and cerebellar hemispheres were 0.011 ± 0.003 and 0.015 ± 0.009 min^{-1} respectively, indicating the tracer has similar dissociation rates for striatum and cerebellar hemisphere. The specificity of binding (k_3/k_4) value for striatum (3.7) was over 3-fold greater than for the cerebellar hemispheres (1.3), which is consistent with enrichment of VAChT in the striatum. The V_T values derived from $K_1/k_2 \cdot (1+k_3/k_4)$ for striatum and cerebellar hemispheres were 9.5 ± 1.6 and 3.3 ± 1.1 mL g^{-1} respectively, which confirmed further ~ 3-fold greater uptake of (–)-[11C]**TZ659** in striatum than in the cerebellar hemispheres. Values of V_T were also derived from Logan graphic analysis with metabolite corrected arterial blood input function. The Logan plot V_T values for striatum and cerebellar hemispheres were 8.8 ± 2.0 and 3.9 ± 1.6 mL·g^{-1} respectively, confirming that the uptake of (–)-[11C]**TZ659** in the striatum was > 2-fold greater than uptake in the cerebellar hemispheres (Table 1).

To evaluate the applicability of reference tissue methods that have been widely reported to produce more stable and reliable modeling without collecting arterial blood samples, PET data were also analyzed using SRTM and LoganREF methods. For the six baseline scans (including four from Subject A and two from Subject B), the striatal BP_{ND} calculated with LoganREF using cerebellar hemisphere as the reference region (1.5 ± 0.26) was identical to the corresponding striatal BP_{ND} value using SRTM (1.5 ± 0.12, Table 2). In the SRTM modeling the rate constant for transfer of tracer from striatum to plasma (k_2) and rate constant ratio between striatum and cerebellar hemispheres ($R_1 = K_1/K_1' = k_2/k_2'$) were also estimated. The k_2 averaged across all six baseline scans for striatum was 0.055 ± 0.034 min^{-1} (Table 2) and R_1 averaged all six baseline was 0.75 ± 0.090 for striatum (Table 2). Therefore the rate constant for transfer of tracer from cerebellum to plasma (k_2') can be estimated by the equation: $k_S' = k_2 / R_1$. Using SRTM estimates of k_2 and R_1 for baseline scans (Table 2), the calculated range of k_2' was 0.029 – 0.13 min^{-1}, which is consistent with the cerebellum k_2 estimate of 0.11 ± 0.03 min^{-1} from 2TCM modeling with arterial blood input function (Table 1).

3.3. Pharmacological pretreatment and displacement experiments

The regional TACs are presented in Figure 2. The tissue concentration of (–)-[11C]**TZ659** peaked ~ 20 min p.i. and was followed by a relatively high retention in the target striatal regions, with rapid washout from cerebellar hemispheres. The regional TACs revealed that uptake of (–)-[11C]**TZ659** in the striatum, but not in the cerebellar hemispheres, was

reduced following pretreatment with increasing doses of (−)-vesamicol 6 min prior to tracer injection. Initial cerebellar and striatal uptake in the blocking study was higher than the average uptake during the initial period in the baseline studies; this may result from variability associated with the scan, for example, differences in the rate of the bolus injection between studies, the minor differences in the interval between the administering the initial anesthetic and radiotracer injection, or differences in the depth of anesthesia; in addition, (−)-vesamicol that was reported to have high toxicity [44, 45], for blocking studies, another potential explanation is that the difference may be caused by a pharmacological response to the potent inhibitor (−)-vesamicol. Despite the difference seen in initial uptake, the steady state retention of the tracer in the cerebellum (after 70 min post injection of the radiotracer) did not change following pretreatment with (−)-vesamicol. The baseline data shown in Figure 2 were averaged from four scans in the NHP Subject A; the blocking and baseline curves for cerebellar hemisphere almost overlap by 70 min p.i. (Figure 2), suggesting that the cerebellar hemisphere can serve as a reference region for VAChT under both baseline and vesamicol blocking conditions. A dose of 0.05 mg/kg (−)-vesamicol resulted in a 56% decrease in the striatum: cerebellar hemispheres ratio 20-min post-injection, indicated by SUV. Pretreatment with 0.25 mg/kg (−)-vesamicol decreased tracer binding by 72%; with a clear dose-dependent reduction in radiotracer accumulation observed following pretreatment with increasing doses of (−)-vesamicol (Figure 2, Table 2). LoganREF analysis also was applied to baseline data and showed regionally specific uptake with striatum > thalamus > frontal cortex > hippocampus > occipital cortex > temporal cortex > midbrain (Figure 3A). Although this uptake ranking order was similar after pretreatment with (−)-vesamicol at 0.25 mg/kg, striatal retention of (−)-[^{11}C]**TZ659** decreased dramatically in the blocking study (Figure 3B), consistent with the change in BP_{ND} values shown in Table 2. Displacement of the radiotracer from the striatum was observed when (−)-vesamicol (0.3 mg/kg) was injected 20 min after (−)-[^{11}C]**TZ659** administration (Figure 4). The striatal SUV for (−)-[^{11}C]**TZ659** decreased quickly after administration of (−)-vesamicol; by the end of the 120 min scan, tracer uptake in the striatum had decreased by 50% and approached levels in the cerebellar hemispheres. These results demonstrate that (−)-[^{11}C]**TZ659** has reversible binding to VAChT.

3.4. Occupancy studies

The data acquired from the (−)-vesamicol pretreatment studies were used to determine the target occupancy following administration of different doses and to estimate the *in vivo* affinity of the ligand for the VAChT. In pharmacological studies, the dose at which 50% of the maximal effect observed is the ED_{50}. A radiotracer for VAChT with selective, reversible binding could be used in this way to quantify the binding site occupancy of other VAChT ligands or for the noninvasive measurement of changes in VAChT expression following pharmacological treatments that target cholinergic systems. The BP_{ND} values (both from LoganREF and SRTM for occupancy studies) are presented in Table 2. These data suggest that BP_{ND} values are reduced by escalating doses of (−)-vesamicol. The (−)-vesamicol occupancy levels obtained were 55%, 56%, 78% and 72% for LoganREF (BP_{ND}); 44%, 60%, 77%, and 75% for SRTM (BP_{ND}) occupancy plot analysis, BP_{ND} values are shown for (−)-vesamicol doses of 0.01, 0.05, 0.125, and 0.25 mg/kg, respectively. The scatter plot of striatal BP_{ND} with SRTM modeling versus BP_{ND} LoganREF modeling showed good

correlation ($r_2 = 0.97$), this plot includes data from six baseline studies (circles) and four escalating doses of (−)-vesamicol, one (+)-pentazocine pretreatment and one S-(−)-eticlopride pretreatment (triangles) (Figure 5A). The excellent agreement between two different modeling approaches suggested that both methods properly reflect *in vivo* specificity of (−)-[11C]**TZ659**. The occupancy percentages for each (−)-vesamicol dose were averaged from two modeling methods (SRTM and LoganREF). Using the four escalating doses of (−)-vesamicol and control (zero point), the fitted ED_{50} of (−)-vesamicol for VAChT was 0.0057 ± 0.002 mg/kg (Figure 5B).

4. Discussion

The newly developed PET tracer (−)-[11C]**TZ659** demonstrated excellent *in vivo* binding specificity to VAChT. This new radiotracer has several advantages compared to others for quantifying cholinergic activities *in vivo*. First, high potency and selectivity for VAChT makes (−)-[11C]**TZ659** a superb radioligand for quantifying cholinergic presynaptic terminals [27, 28]. Second, this study and our previous studies revealed that this tracer has highly specific uptake in the VAChT-enriched striatum while the cerebellar hemisphere reference region appears devoid of specific binding sites. The reference region of cerebellum was properly defined by excluding the cerebellum-vermis which has shown VAChT *in vivo* binding [24]. Our blocking studies further confirmed uptake of (−)-[11C]**TZ659** in the cerebellar hemisphere under baseline conditions and in the blocking study using (−)-vesamicol pretreatment (0.25 mg/kg) displayed a similar steady state TAC profile by 70 min p.i. (Figure 2) although the initial uptake in the blocking study showed some variability. For the displacement study using 0.3 mg/kg of (−)-vesamicol administered during steady-state, variability in initial uptake was minor; more importantly, the TACs for cerebellar hemisphere uptake following injection of (−)-vesamicol 20 min p.i. compared with the baseline TAC for the cerebellar hemisphere (Figure 4) showed great similarity. These studies confirmed that the cerebellum is the proper reference region. Third, the studies reported herein demonstrate that (−)-[11C]**TZ659** binds reversibly in striatum to VAChT with advantageous kinetics.

For many years, [123I]-IBVM ((±)-*trans*-2-hydroxy-3-[4-(3-iodophenyl)piperidyl]-1,2,3,4-tetrahydronaphthalene) has been used clinically to assess the level of VAChT, but lengthy image acquisition may limit its applications. Furthermore, previous studies revealed that sigma receptor ligands can block the uptake of [123I]-IBVM which suggested that [123I]-IBVM may cross bind to sigma receptors [46]. The radiation dosimetry of the 18F-labeled benzovesamicol analogue, [18F]fluoroethoxy-benzovesamicol ([18F]FEOBV) and kinetic modeling for assessing VAChT levels in human brain was recently reported [24]. [18F]FEOBV offers advantages over SPECT ligands for both preclinical and clinical imaging of cholinergic loss. Studies of [18F]FEOBV in a rat model of cholinergic dysfunction showed a good correlation between PET measurements of [18F]FEOBV uptake and *ex vivo* autoradiography in the same animals [47]. However, equilibrium kinetics of [18F]FEOBV in the brain of both NHP and human subjects suggest that it requires more than 360 min p.i. to reach steady state [24, 48]. This may cause challenges for clinical studies with [18F]FEOBV in patients with impaired cognitive function. Our recent *in vitro* pharmacological evaluation of the tritiated counterpart of (−)-[3H]**TZ659** showed that it has

high affinity (K_d = 1.97 nM) and specificity for VAChT [28]. Here, we further demonstrated the *in vivo* binding selectivity and specificity of (−)-[11C]**TZ659** toward VAChT in NHPs, its reversible binding property, and its suitable radiopharmaceutical kinetics. These results warrant clinical evaluation of (−)-[11C]**TZ659** in human subjects.

In the microPET baseline scans, (−)-[11C]**TZ659** readily entered the brain and showed a heterogeneous distribution. Striatum demonstrated the highest accumulation with good retention of radioactivity; consistent with reported *in vitro* immunohistochemistry indicating the highest concentration of VAChT in striatum [49–51]. Slow uptake and washout have hampered the advance of other radioligands for clinical imaging studies of VAChT; rapid kinetics is an important feature for PET imaging studies of the CNS [52]. The TAC for (−)-[11C]**TZ659** under baseline conditions revealed a comparatively rapid uptake and peak striatal equilibration with more rapid washout from non-target regions, particularly the cerebellar hemispheres (Figure 2, 4). A peak of striatal uptake was reached ~ 20 min p.i.; the tracer was retained for 30–40 min, then slowly washed out. As indicated in Table 2 and Figure 5, the SRTM BP_{ND} estimate correlated well with the estimates obtained from LoganREF plots. Kinetics modeling using 2TCM and Logan plot analyses showed a significantly high ratio of V_T striatum-to-cerebellum ratio (~3) (Tables 1 and 2). These modeling studies collectively and consistently reveal the suitability of [11C]**TZ659** for assessing VAChT *in vivo*. Our studies also suggested that referenced based modeling (SRTM, LoganREF) without blood sampling provided consistent results when compared with kinetic modeling (2TCM and Logan analysis) using arterial blood input functions.

The *in vivo* specificity of (−)-[11C]**TZ659** binding to VAChT in the NHP brain was supported by reductions in striatal uptake following administration of (−)-vesamicol either pre- or post-tracer injection. Furthermore, the observed displacement of striatal radioactivity post injection of (−)-vesamicol confirmed that binding of (−)-[11C]**TZ659** to VAChT is reversible. No effect was observed on tracer kinetics by pretreatment of the animal with (+)-pentazocine, a known sigma-1 ligand, suggesting (−)-**TZ659** has negligible binding to the sigma-1 receptor. These results are consistent with our previously reported data [27, 28]. In comparison, pretreatment of the NHP subject with the D_2-like receptor antagonist S-(−)-eticlopride increased the BP_{ND} of (−)-[11C]**TZ659** (BP_{ND} = 2.6 and 2.7, with LoganREF and SRTM respectively Table 2). The result was consistent with previous reports that S-(−)-eticlopride stimulated binding in rats of a SPECT ligand for VAChT [43]. Another D_2–like receptor antagonist, haloperidol, has been similarly reported as markedly augmenting uptake of the aminobenzovesamicol PET tracer (−)-[18F]NEFA in NHP [53]. Our *in vitro* binding data showed that the binding of (−)-[3H]**TZ659** to VAChT is not affected by S-(−)-eticlopride in the post-nuclear supernatant of a stably transfected PC12[A123.7] cell line that expresses human VAChT [28]. This lack of agreement between the *in vitro* and the *in vivo* findings may be attributed to the interaction of cholinergic and dopaminergic systems in the living brain (Figure 6). Activation of nicotinic acetylcholine receptors (nAChRs) by ACh facilitates dopamine release in the striatum [54]. In contrast, the predominant effect of dopaminergic activation is suppression of ACh release, which is mediated by D_2–like receptors [55]. S-(−)-eticlopride is an antagonist for D_2–like receptors, hence eticlopride-induced down-regulation of dopaminergic output could enhance ACh release [56]. This

phenomenon could be used to measure the so-called "cholinergic reserve" [13] with PET using VAChT radiotracers such as (–)-[11C]**TZ659** in healthy young and aged subjects and promote the development of new cholinergic therapies.

(–)-[11C]**TZ659** was also used to calculate the degree of VAChT binding site occupancy produced by pretreatment of a NHP with escalating doses of (–)-vesamicol. A dose of approximately 0.0057 mg/kg (–)-vesamicol was estimated to produce 50% VAChT occupancy in the striatum. These results provided an example to estimate the degree of VAChT occupancy under pharmacological intervention, and they provided essential information on the pharmacokinetic-pharmacodynamics relationship of (–)-vesamicol [57].

High striatal uptake of (–)-[11C]**TZ659** permits *in vivo* measurement of striatal cholinergic function. The striatum is a prominent site for cholinergic neuropathology in several neurodegenerative diseases, including Huntington's disease (HD) and PD. For instance, both mRNA and protein levels of VAChT are decreased significantly in the striatum of a HD transgenic mouse model [58]. VAChT expression also was downregulated by 51.4% in the striatum of HD patients, compared with a control group [58]. In PD, an imbalance of acetylcholine and dopamine may contribute to clinical symptoms. Dopamine depletion blocks autoinhibition of acetylcholine release, leading to excessive acetylcholine release that eventually interrupts information transfer from motor command centers in the cerebral cortex [59]. Therefore, VAChT could serve as a useful biomarker for diseases involving loss of striatal cholinergic neurons, and noninvasive PET imaging with (–)-[11C]**TZ659** could be used to monitor disease progression and therapeutic effects using a cholinergic inhibition strategy.

5. Conclusion

(–)-[11C]**TZ659** is a promising PET radiotracer that can be used to investigate VAChT. The high retention of (–)-[11C]**TZ659** in the striatum could be either prevented or displaced in a dose dependent manner by (–)-vesamicol. D_2–like antagonism resulted in increased striatal uptake of (–)-[11C]**TZ659**, which could be used for *in vivo* investigation of the relationship between the dopaminergic and cholinergic systems. Further investigation of (–)-[11C]**TZ659** in animal models and translational clinical investigations are warranted to determine if it is a suitable tracer for quantifying the VAChT levels in human subjects and determine its utility in measuring changes in VAChT expression during disease progression or therapeutic treatment with cholinergic inhibitors.

Acknowledgment

Abbreviation list

ACh	acetylcholine
AChE	acetylcholinesterase
AD	Alzheimer's disease
AIR	automated image registration
BP_{ND}	binding potential (non-displaceable)
ChAT	choline acetyltransferase
CNS	central nervous system
C_R	radiotracer concentration in the reference region
C_T	radiotracer concentration in the target region
EOB	end of bombardment
DVR	distribution volume ratio
$[^{18}F]$-FEOBV	(−)-5-^{18}F-fluoroethoxybenzovesamicol
HD	Huntington's disease
HPLC	high-performance liquid chromatography
i.v.	intravenous injection
K_1	transfer constant from plasma to specific target tissue (mL g^{-1} min^{-1})
k_2	transfer constant from tissue to plasma (min $^{-1}$)
k_3	association constant for ligand-binding site (min $^{-1}$)
k_4	dissociation constant for ligand-binding site (min $^{-1}$)
K_d	dissociation constant
LoganREF	Logan Reference
MP-RAGE	magnetization-prepared rapid gradient-echo
nAChR	nicotinic acetylcholine receptor
NHP	nonhuman primate
Occ	target occupancy
PD	Parkinson's disease
PET	positron emission tomography
p.i.	post injection
ROI	region of interest
SPECT	single-photon emission computed tomography
SRTM	simplified reference tissue model

SD	standard deviation
SUV	standardized uptake value
TAC	time activity curve
2TCM	two-tissue compartment model
VAChT	vesicular acetylcholine transporter
V_T	volume of distribution

References

1. Bartus RT, Dean RL, Beer B, Lippa AS. The cholinergic hypothesis of geriatric memory dysfunction. Science. 1982; 217:408–414. [PubMed: 7046051]

2. Bartus RT, Dean RL, Pontecorvo MJ, Flicker C. The cholinergic hypothesis: A historical overview, current perspective, and future directions. Ann N Y Acad Sci. 1985; 444:332–358. [PubMed: 2990293]

3. Contestabile A. The history of the cholinergic hypothesis. Behav Brain Res. 2011; 221:334–340. [PubMed: 20060018]

4. Davis KL, Mohs RC, Marin D, Purohit DP, Perl DP, Lantz M, et al. Cholinergic markers in elderly patients with early signs of Alzheimer disease. JAMA. 1999; 281:1401–1406. [PubMed: 10217056]

5. DeKosky ST, Ikonomovic MD, Styren SD, Beckett L, Wisniewski S, Bennett DA, et al. Upregulation of choline acetyltransferase activity in hippocampus and frontal cortex of elderly subjects with mild cognitive impairment. Ann Neurol. 2002; 51:145–155. [PubMed: 11835370]

6. Dumas JA, Newhouse PA. The cholinergic hypothesis of cognitive aging revisited again: Cholinergic functional compensation. Pharmacol Biochem Behav. 2011; 99:254–261. [PubMed: 21382398]

7. Terry AV Jr, Buccafusco JJ. The cholinergic hypothesis of age and Alzheimer's disease-related cognitive deficits: Recent challenges and their implications for novel drug development. J Pharmacol Exp Ther. 2003; 306:821–827. [PubMed: 12805474]

8. Varoqui H, Erickson JD. Active transport of acetylcholine by the human vesicular acetylcholine transporter. J Biol Chem. 1996; 271:27229–27232. [PubMed: 8910293]

9. Arvidsson U, Riedl M, Elde R, Meister B. Vesicular acetylcholine transporter (VAChT) protein: A novel and unique marker for cholinergic neurons in the central and peripheral nervous systems. J Comp Neurol. 1997; 378:454–467. [PubMed: 9034903]

10. Bravo DT, Kolmakova NG, Parsons SM. Choline is transported by vesicular acetylcholine transporter. J Neurochem. 2004; 91:766–768. [PubMed: 15485505]

11. Prado VF, Roy A, Kolisnyk B, Gros R, Prado MA. Regulation of cholinergic activity by the vesicular acetylcholine transporter. Biochem J. 2013; 450:265–274. [PubMed: 23410039]

12. Usdin TB, Eiden LE, Bonner TI, Erickson JD. Molecular biology of the vesicular ACh transporter. Trends Neurosci. 1995; 18:218–224. [PubMed: 7610492]

13. Efange SM. In vivo imaging of the vesicular acetylcholine transporter and the vesicular monoamine transporter. FASEB J. 2000; 14:2401–2413. [PubMed: 11099458]

14. Giboureau N, Som IM, Boucher-Arnold A, Guilloteau D, Kassiou M. PET radioligands for the vesicular acetylcholine transporter (VAChT). Curr Top Med Chem. 2010; 10:1569–1583. [PubMed: 20583990]

15. Khare P, Ojeda AM, Chandrasekaran A, Parsons SM. Possible important pair of acidic residues in vesicular acetylcholine transporter. Biochemistry. 2010; 49:3049–3059. [PubMed: 20225888]

16. Khare P, Mulakaluri A, Parsons SM. Search for the acetylcholine and vesamicol binding sites in vesicular acetylcholine transporter: The region around the lumenal end of the transport channel. J Neurochem. 2010; 115:984–993. [PubMed: 20831599]

17. Lamare F, Mazere J, Attila M, Mayo W, De Clermont-Gallerande H, Meissner W, et al. Improvement of in vivo quantification of [123I]-iodobenzovesamicol in single-photon emission computed tomography/computed tomography using anatomic image to brain atlas nonrigid registration. Mol Imaging. 2013; 12:288–299. [PubMed: 23759370]

18. Tu Z, Wang W, Cui J, Zhang X, Lu X, Xu J, et al. Synthesis and evaluation of in vitro bioactivity for vesicular acetylcholine transporter inhibitors containing two carbonyl groups. Bioorg Med Chem. 2012; 20:4422–4429. [PubMed: 22739089]

19. Tu Z, Efange SM, Xu J, Li S, Jones LA, Parsons SM, et al. Synthesis and in vitro and in vivo evaluation of 18F-labeled positron emission tomography (PET) ligands for imaging the vesicular acetylcholine transporter. J Med Chem. 2009; 52:1358–1369. [PubMed: 19203271]

20. Bergman S, Estrada S, Hall H, Rahman R, Blomgren A, Larhed M, et al. Synthesis and labeling of a piperazine-based library of 11C-labeled ligands for imaging of the vesicular acetylcholine transporter. J Labelled Comp Radiopharm. 2014; 57:525–532. [PubMed: 24991704]

21. Parent MJ, Bedard MA, Aliaga A, Minuzzi L, Mechawar N, Soucy JP, et al. Cholinergic depletion in Alzheimer's disease shown by [18F]FEOBV autoradiography. Int J Mol Imaging. 2013; 2013:205045. [PubMed: 24324884]

22. Sorger D, Scheunemann M, Vercouillie J, Grossmann U, Fischer S, Hiller A, et al. Neuroimaging of the vesicular acetylcholine transporter by a novel 4-[18F]fluoro-benzoyl derivative of 7-hydroxy-6-(4-phenylpiperidin-1-yl)-octahydro-benzo[1,4]oxazines. Nucl Med Biol. 2009; 36:17–27. [PubMed: 19181265]

23. Scheunemann M, Sorger D, Wenzel B, Heinitz K, Schliebs R, Klingner M, et al. Synthesis of novel 4- and 5-substituted benzyl ether derivatives of vesamicol and in vitro evaluation of their binding properties to the vesicular acetylcholine transporter site. Bioorg Med Chem. 2004; 12:1459–1465. [PubMed: 15018919]

24. Petrou M, Frey KA, Kilbourn MR, Scott PJ, Raffel DM, Bohnen NI, et al. In vivo imaging of human cholinergic nerve terminals with (-)-5-18F-fluoroethoxybenzovesamicol: Biodistribution, dosimetry, and tracer kinetic analyses. J Nuc Med. 2014; 55:396–404.

25. Padakanti PK, Zhang X, Li J, Parsons SM, Perlmutter JS, Tu Z. Syntheses and radiosyntheses of two carbon-11 labeled potent and selective radioligands for imaging vesicular acetylcholine transporter. Mol Imaging Biol. 2014; 16:765–772. [PubMed: 24875230]

26. Padakanti PK, Zhang X, Jin H, Cui J, Wang R, Li J, et al. In vitro and in vivo characterization of two C-11-labeled PET tracers for vesicular acetylcholine transporter. Mol Imaging Biol. 2014; 16:773–780. [PubMed: 24865402]

27. Li J, Zhang X, Zhang Z, Padakanti PK, Jin H, Cui J, et al. Heteroaromatic and aniline derivatives of piperidines as potent ligands for vesicular acetylcholine transporter. J Med Chem. 2013; 56:6216–6233. [PubMed: 23802889]

28. Liu H, Jin H, Li J, Zhang X, Kaneshige K, Parsons SM, et al. In vitro and ex vivo characterization of (-)-TZ659 as a ligand for imaging the vesicular acetylcholine transporter. Eur J Pharmacol. 2015; 752:18–25. [PubMed: 25678250]

29. Tu Z, Zhang X, Jin H, Yue X, Padakanti PK, Yu L, et al. Synthesis and biological characterization of a promising F-18 PET tracer for vesicular acetylcholine transporter. Bioorg Med Chem. 2015; 23:4699–4709. [PubMed: 26138195]

30. Liu H, Jin H, Yue X, Zhang X, Yang H, Li J, et al. Preclinical evaluation of a promising C-11 labeled PET tracer for imaging phosphodiesterase 10A in the brain of living subject. Neuroimage. 2015; 121:253–262. [PubMed: 26216275]

31. Fan J, Zhang X, Li J, Jin H, Padakanti PK, Jones LA, et al. Radiosyntheses and in vivo evaluation of carbon-11 PET tracers for PDE10A in the brain of rodent and nonhuman primate. Bioorg Med Chem. 2014; 22:2648–2654. [PubMed: 24721831]

32. Fowler SC, Liou JR. Haloperidol, raclopride, and eticlopride induce microcatalepsy during operant performance in rats, but clozapine and SCH 23390 do not. Psychopharmacology (Berl). 1998; 140:81–90. [PubMed: 9862406]

33. White IM, Rebec GV. Performance on a lever-release, conditioned avoidance response task involves both dopamine D_1 and D_2 receptors. Eur J Pharmacol. 1994; 253:167–169. [PubMed: 8013542]

34. Miller TR, Wallis JW, Wilson AD. Interactive reconstruction in single-photon tomography. Eur J Nucl Med. 1989; 15:189–193. [PubMed: 2787746]

35. Tabbal SD, Mink JW, Antenor JA, Carl JL, Moerlein SM, Perlmutter JS. 1-Methyl-4-phenyl-1,2,3,6-tetrahydropyridine-induced acute transient dystonia in monkeys associated with low striatal dopamine. Neuroscience. 2006; 141:1281–1287. [PubMed: 16766129]

36. Woods RP, Mazziotta JC, Cherry SR. MRI-PET registration with automated algorithm. J Comput Assist Tomogr. 1993; 17:536–546. [PubMed: 8331222]

37. Koeppe RA, Holthoff VA, Frey KA, Kilbourn MR, Kuhl DE. Compartmental analysis of [^{11}C]flumazenil kinetics for the estimation of ligand transport rate and receptor distribution using positron emission tomography. J Cereb Blood Flow Metab. 1991; 11:735–744. [PubMed: 1651944]

38. Logan J, Fowler JS, Volkow ND, Wolf AP, Dewey SL, Schlyer DJ, et al. Graphical analysis of reversible radioligand binding from time-activity measurements applied to [N-^{11}C-methyl]-(-)-cocaine PET studies in human subjects. J Cereb Blood Flow Metab. 1990; 10:740–747. [PubMed: 2384545]

39. Innis RB, Cunningham VJ, Delforge J, Fujita M, Gjedde A, Gunn RN, et al. Consensus nomenclature for in vivo imaging of reversibly binding radioligands. J Cereb Blood Flow Metab. 2007; 27:1533–1539. [PubMed: 17519979]

40. Lammertsma AA, Hume SP. Simplified reference tissue model for PET receptor studies. Neuroimage. 1996; 4:153–158. [PubMed: 9345505]

41. Watabe H, Itoh M, Cunningham V, Lammertsma AA, Bloomfield P, Mejia M, et al. Noninvasive quantification of rCBF using positron emission tomography. J Cereb Blood Flow Metab. 1996; 16:311–319. [PubMed: 8594064]

42. Suhara T, Takano A, Sudo Y, Ichimiya T, Inoue M, Yasuno F, et al. High levels of serotonin transporter occupancy with low-dose clomipramine in comparative occupancy study with fluvoxamine using positron emission tomography. Arch Gen Psychiatry. 2003; 60:386–391. [PubMed: 12695316]

43. Efange SM, Langason RB, Khare AB. Age-related diminution of dopamine antagonist-stimulated vesamicol receptor binding. Journal of Nuclear Medicine. 1996; 37:1192–1197. [PubMed: 8965197]

44. Rogers GA, Parsons SM, Anderson DC, Nilsson LM, Bahr BA, Kornreich WD, et al. Synthesis, in vitro acetylcholine-storage-blocking activities, and biological properties of derivatives and analogues of trans-2-(4-phenylpiperidino)cyclohexanol (vesamicol). J Med Chem. 1989; 32:1217–1230. [PubMed: 2724295]

45. Kilbourn MR. PET radioligands for the vesicular transporters for monoamines and acetylcholine. J Labelled Comp Radiopharm. 2013; 56:167–171. [PubMed: 24285322]

46. Efange SM, von Hohenberg K, Khare AB, Tu Z, Mach RH, Parsons SM. Synthesis and biological characterization of stable and radioiodinated (±)-*trans*-2-hydroxy-3-{4-(3-iodophenyl)piperidyl}-1,2,3,4-tetrahydronaphthalene (3'-IBVM). Nucl Med Biol. 2000; 27:749–755. [PubMed: 11150707]

47. Kilbourn MR, Hockley B, Lee L, Sherman P, Quesada C, Frey KA, et al. Positron emission tomography imaging of (*2R,3R*)-5-[^{18}F]fluoroethoxybenzovesamicol in rat and monkey brain: A radioligand for the vesicular acetylcholine transporter. Nuc Med Biol. 2009; 36:489–493.

48. Kilbourn, MR.; Hockley, B.; Lee, L.; Koeppe, RA. Neuroimage. Pittsburgh, PA: 2008. Successful [^{18}F]FEOBV imaging of the VAChT in monkey brain; p. T93

49. Gilmor ML, Nash NR, Roghani A, Edwards RH, Yi H, Hersch SM, et al. Expression of the putative vesicular acetylcholine transporter in rat brain and localization in cholinergic synaptic vesicles. J Neurosci. 1996; 16:2179–2190. [PubMed: 8601799]

50. Schafer MK, Weihe E, Erickson JD, Eiden LE. Human and monkey cholinergic neurons visualized in paraffin-embedded tissues by immunoreactivity for VAChT, the vesicular acetylcholine transporter. J Mol Neurosci. 1995; 6:225–235. [PubMed: 8860234]

51. Weihe E, Tao-Cheng JH, Schafer MK, Erickson JD, Eiden LE. Visualization of the vesicular acetylcholine transporter in cholinergic nerve terminals and its targeting to a specific population of small synaptic vesicles. Proc Natl Acad Sci U S A. 1996; 93:3547–3552. [PubMed: 8622973]

52. Laruelle M, Slifstein M, Huang Y. Relationships between radiotracer properties and image quality in molecular imaging of the brain with positron emission tomography. Mol Imaging Biol. 2003; 5:363–375. [PubMed: 14667491]

53. Ingvar M, Stone-Elander S, Rogers GA, Johansson B, Eriksson L, Parsons SM, et al. Striatal D_2/acetylcholine interactions: PET studies of the vesamicol receptor. Neuroreport. 1993; 4:1311–1314. [PubMed: 8260611]

54. Lester DB, Rogers TD, Blaha CD. Acetylcholine-dopamine interactions in the pathophysiology and treatment of CNS disorders. CNS Neurosci Ther. 2010; 16:137–162. [PubMed: 20370804]

55. Benarroch EE. Effects of acetylcholine in the striatum. Recent insights and therapeutic implications. Neurology. 2012; 79:274–281. [PubMed: 22802594]

56. Ikarashi Y, Takahashi A, Ishimaru H, Arai T, Maruyama Y. Regulation of dopamine D_1 and D_2 receptors on striatal acetylcholine release in rats. Brain Res Bull. 1997; 43:107–115. [PubMed: 9205804]

57. Borroni E, Zhou Y, Ostrowitzki S, Alberati D, Kumar A, Hainzl D, et al. Pre-clinical characterization of [^{11}C]R05013853 as a novel radiotracer for imaging of the glycine transporter type 1 by positron emission tomography. Neuroimage. 2013; 75:291–300. [PubMed: 22178811]

58. Smith R, Chung H, Rundquist S, Maat-Schieman ML, Colgan L, Englund E, et al. Cholinergic neuronal defect without cell loss in Huntington's disease. Hum Mol Genet. 2006; 15:3119–3131. [PubMed: 16987871]

59. Aosaki T, Miura M, Suzuki T, Nishimura K, Masuda M. Acetylcholine-dopamine balance hypothesis in the striatum: an update. Geriatr Gerontol Int. 2010; 10(Suppl 1):S148–S157. [PubMed: 20590830]
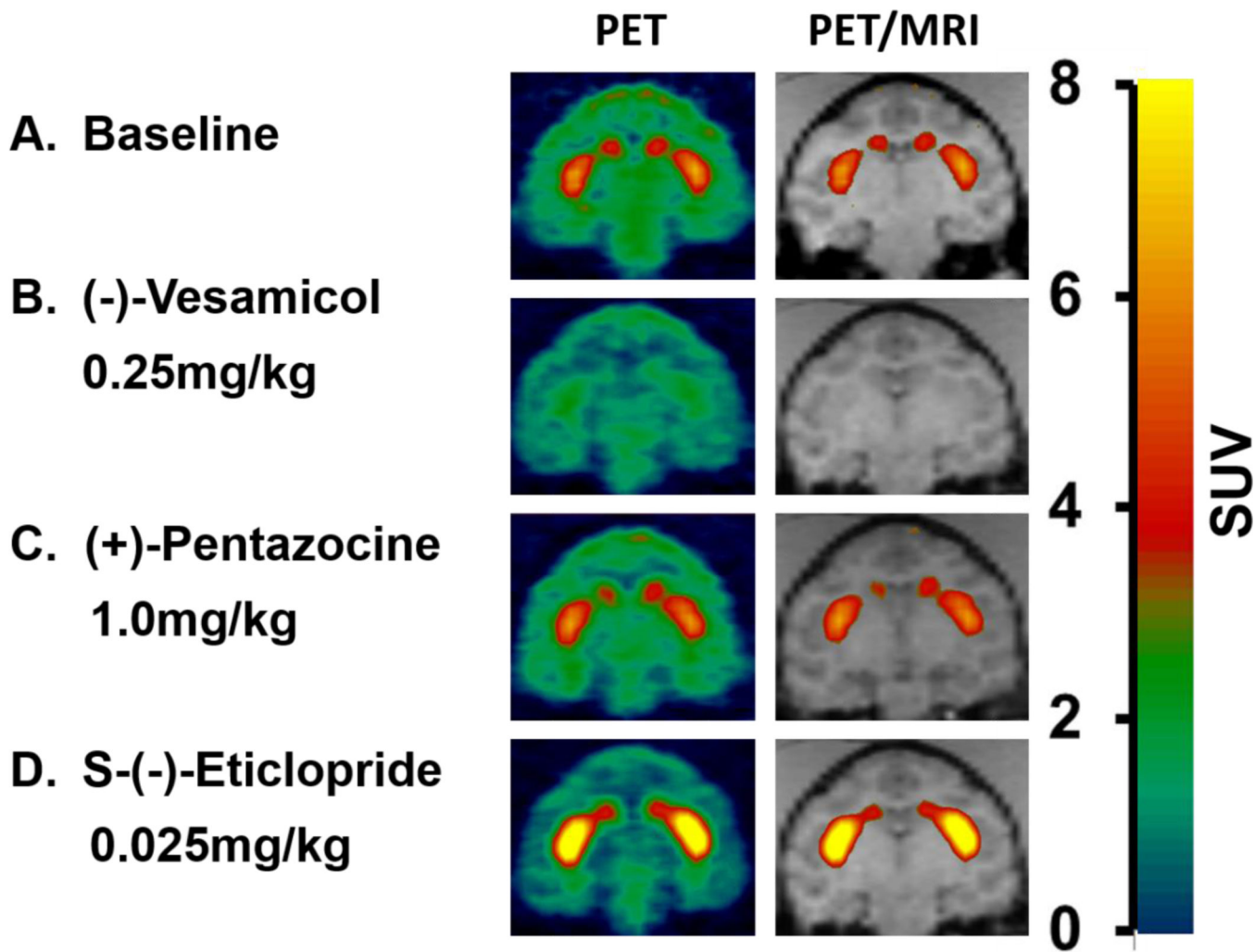
Figure 1. Specificity of (−)-[11C]**TZ659** *in vivo* **binding to VAChT**
Representative coronal images of PET (left) and the coregistered MRI/PET (right) in a male
macaque (Subject A). The baseline scan (**A**) of (−)-[11C]**TZ659** clearly demonstrates striatal
accumulation (caudate and putamen). **B–D** show (−)-[11C]**TZ659** striatal activity after
pretreatment with (**B**) 0.25 mg/kg of the allosteric antagonist (−)-vesamicol; (**C**) 1 mg/kg of
the sigma-1 receptor ligand (+)-pentazocine or (**D**) 0.025 mg/kg of the dopamine D_2-like
receptor antagonist *S*-(−)-eticlopride. Striatal accumulation of (−)-[11C]**TZ659** was
significantly reduced in response to (−)-vesamicol pretreatment, while (+)-pentazocine
pretreatment showed no significant change in striatal activity. D_2–like receptor antagonism
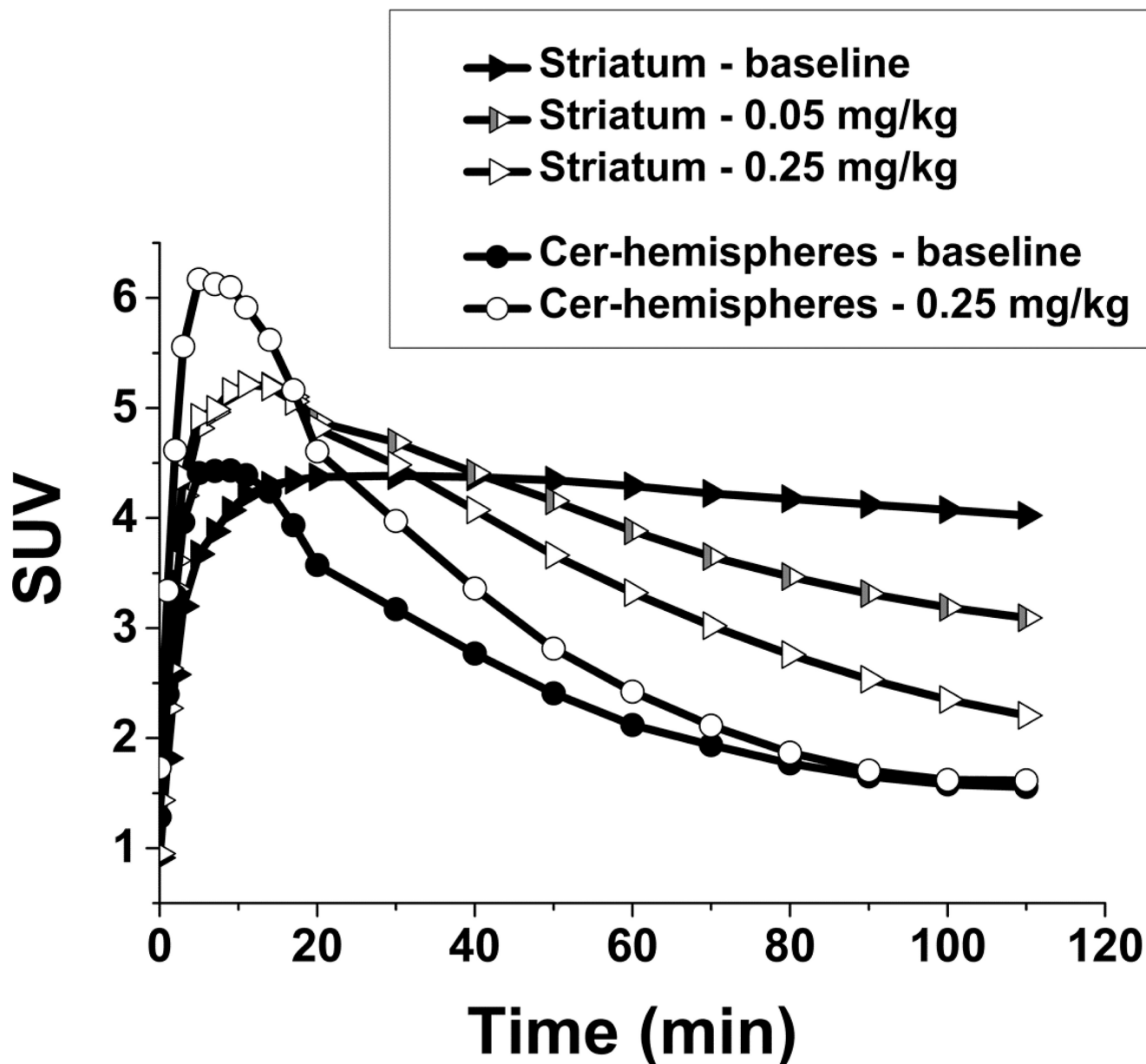with *S*-(−)-eticlopride clearly increased the striatal uptake of the radiotracer.

Figure 2. Cerebellar and striatal time-activity curves (TACs) from baseline and (−)-vesamicol pretreatment (0.25 and 0.05 mg/kg)
Cerebellar TACs at baseline (filled circles) and after (−)-vesamicol treatment (open circles) reached a similar steady state (by 70 min p.i.) although the initial uptake differed; this suggests the cerebellar hemispheres are a suitable non-target reference region. Striatal uptake (combination of caudate and putamen) after pretreatment using 0.05 mg/kg (−)-vesamicol (half-filled triangles) and 0.25 mg/kg (−)-vesamicol (open triangles), was significantly lower than baseline striatal uptake (filled triangles). A greater reduction in striatal uptake during steady state was seen with the higher blocking dose. Baseline data represents the average of all four scans for Subject A.
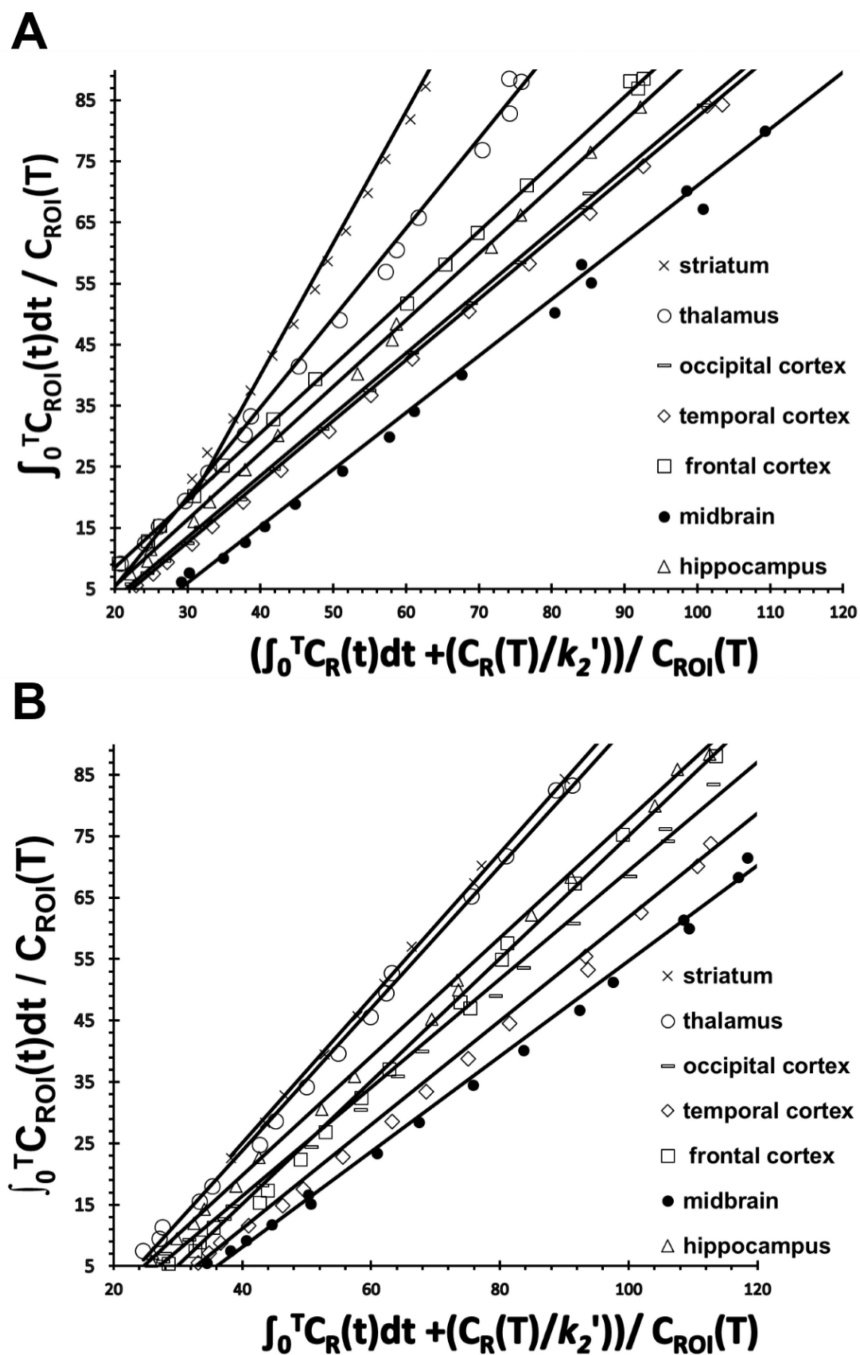
Figure 3. Logan graphic analysis of brain regions

Time activity data for different brain regions (striatum "×", thalamus "○", occipital cortex "−", temporal cortex " ", frontal cortex "□", midbrain "●" and hippocampus " ") for the graphic Logan plots for baseline (A) and experiments with pretreatment by (−)-vesamicol 0.25 mg/kg (B).
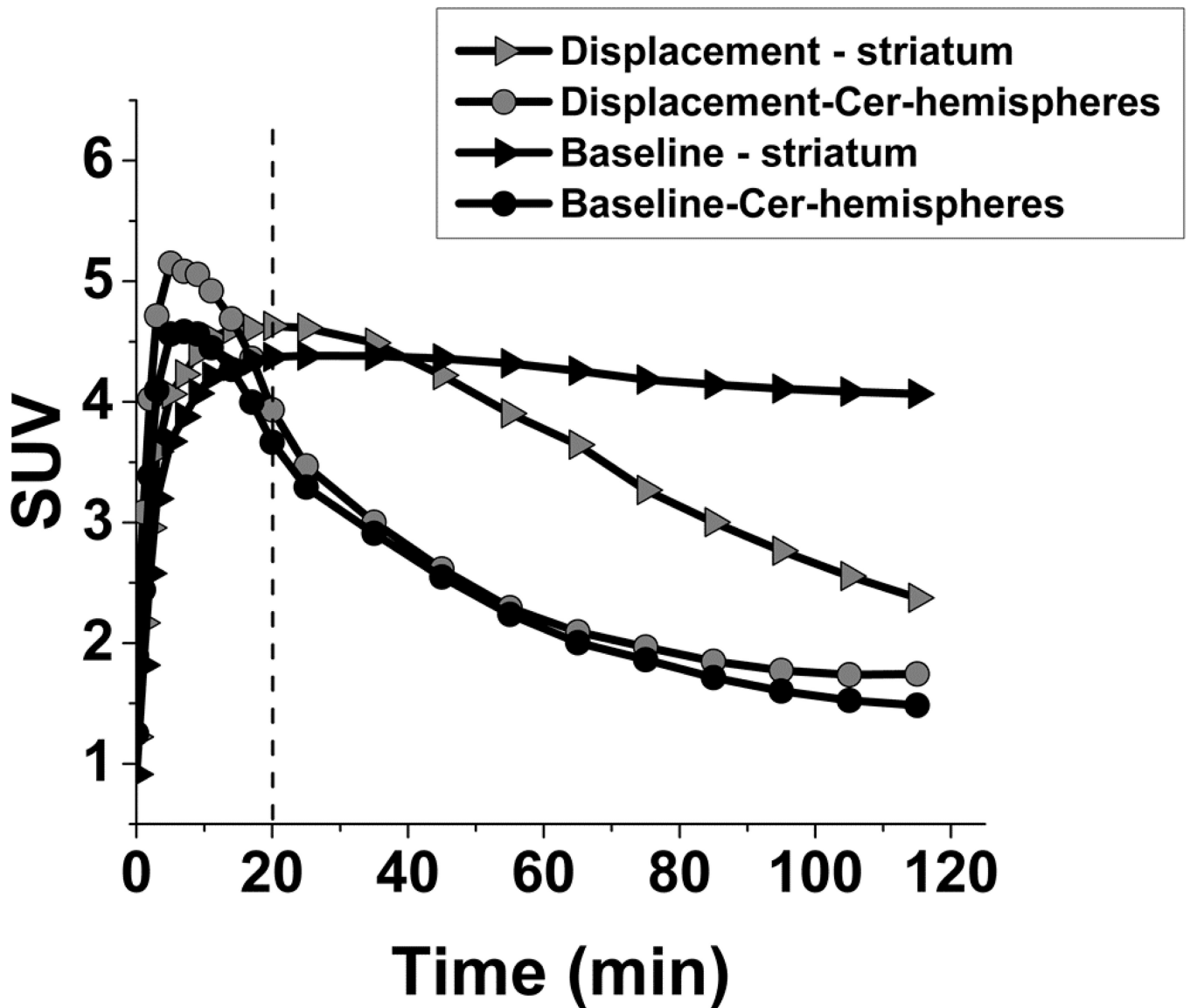
Figure 4. Reversible tracer binding

(−)-Vesamicol (0.3 mg/kg i.v.) was injected 20 min p.i., during striatal equilibrium for displacement studies. Striatal uptake of (−)-[^{11}C]**TZ659** significantly decreased after injection of (−)-vesamicol under displacement conditions (gray triangles) compared to baseline uptake (black triangles). Cerebellar uptake of (−)-[^{11}C]**TZ659** after injection of (−)-vesamicol (grey circles) was almost identical to baseline cerebellar uptake (black circles). Baseline data are the average of all four scans for Subject A.
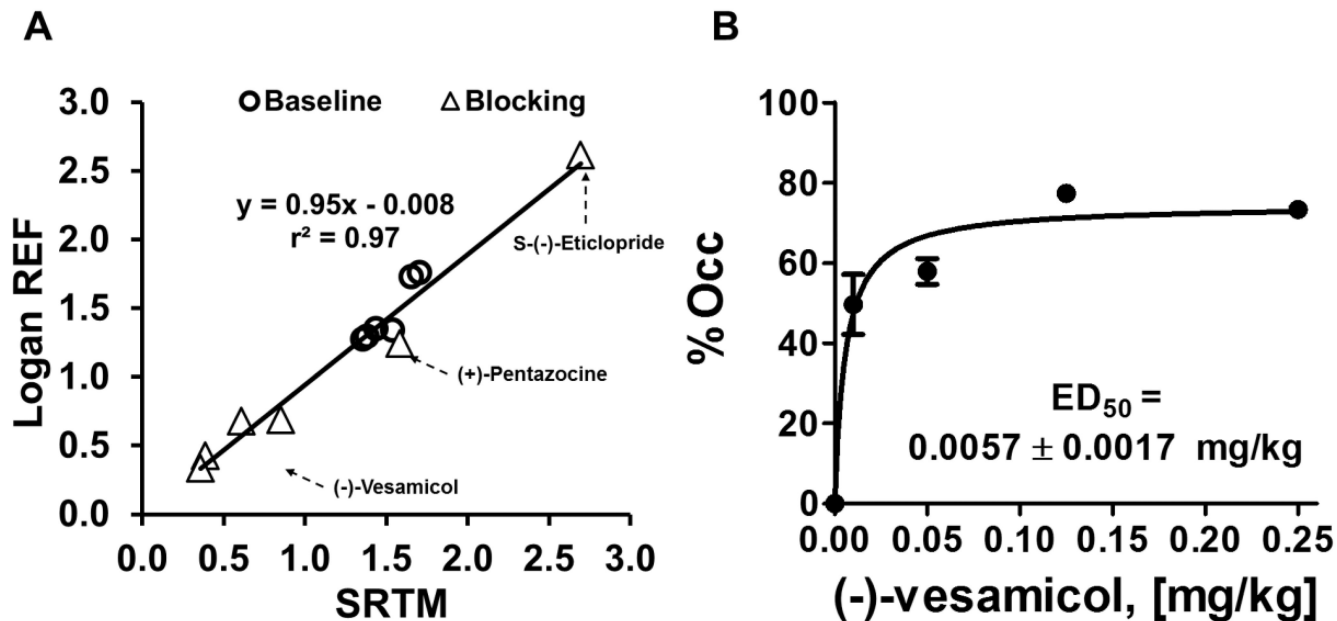
Figure 5. (−)-Vesamicol dose and VAChT occupancy relationship
A) Scatter plot of BP_{ND} estimates with SRTM versus BP_{ND} estimates with LoganREF modeling. Data are for striatal regions under either baseline (circles) or after pretreatment (triangles). All six baseline, four (−)-vesamicol blocking, one (+)-pentazocine blocking, and one *S*-(−)-eticlopride blocking studies are shown. **B).** (−)-Vesamicol dose and VAChT occupancy relationship. The occupancy percentages were calculated from BP_{ND}. The fitted ED_{50} is 0.0057 ± 0.0017 mg/kg.
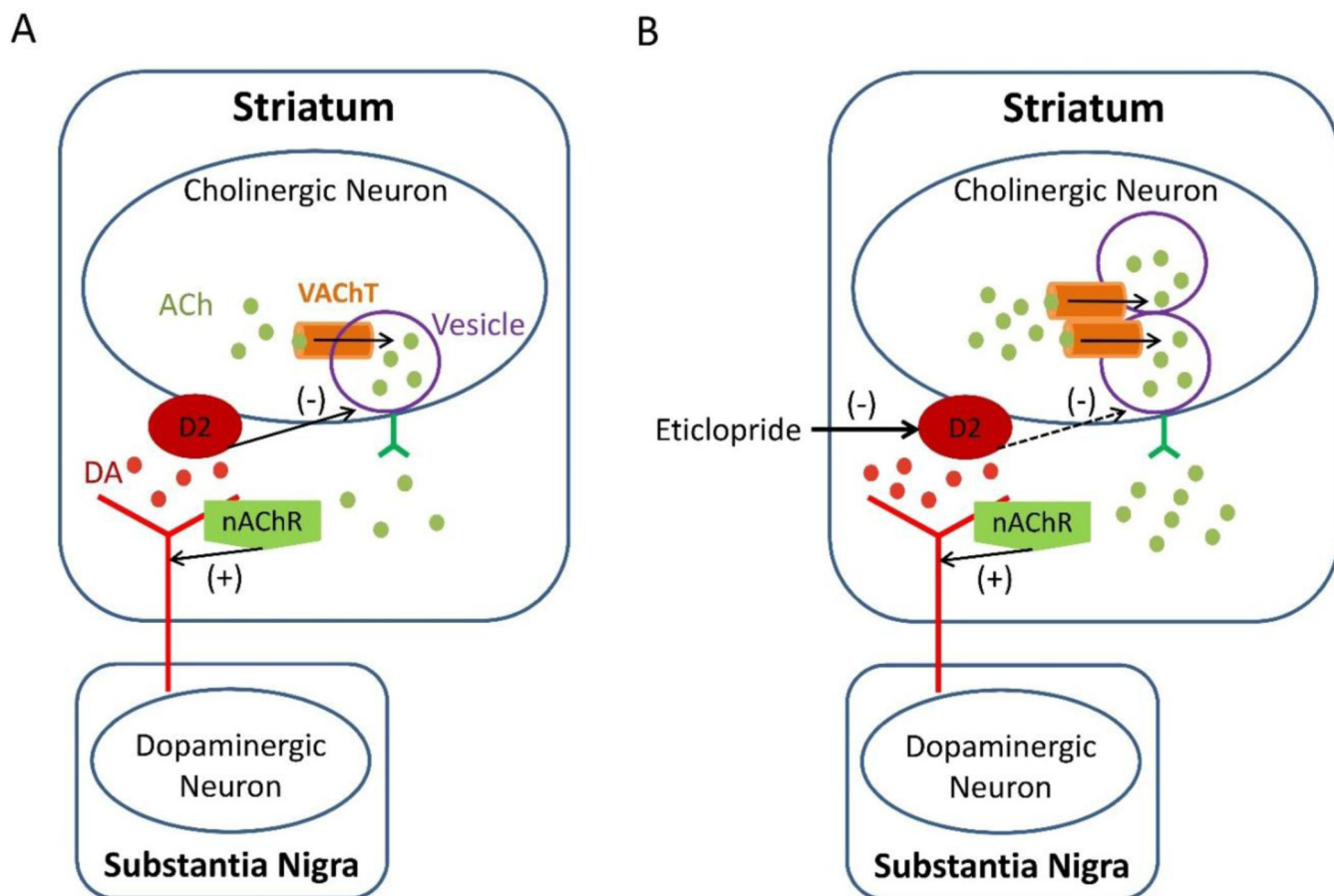
Figure 6. Simplified circuitry cartoon showing the interaction between cholinergic and dopaminergic system in the striatum

A). Acetylcholine (ACh) activation of nicotinic receptors (nAChRs) facilitates dopamine release in the striatum. In contrast, the predominant effect of dopamine is suppression of ACh release, mediated by D_2-like receptors. **B).** S-(−)-eticlopride is an antagonist for D_2-like receptors and therefore down-regulates the consequences for activation of dopaminergic output and enhances cholinergic activity.

Table 1

Kinetic parameters estimates for (−)-[^{11}C]TZ659 from two-tissue compartment modeling and Logan graphic plot with arterial blood input function[*]

| ROIs | Two-tissue compartment modeling (2TCM) | | | | | Logan plot |
	K_1 (mL·g^{-1}·min^{-1})	k_2 (min^{-1})	k_3 (min^{-1})	k_4 (min^{-1})	V_T[**] (mL·g^{-1})	V_T[***] (mL·g^{-1})
Striatum	0.18 ± 0.05	0.052 ± 0.02	0.041 ± 0.006	0.011 ± 0.003	9.5 ± 1.6	8.8 ± 2.0
Cerebellar hemispheres	0.23 ± 0.05	0.11 ± 0.03	0.019 ± 0.001	0.015 ± 0.009	3.3 ± 1.1	3.9 ± 1.6

[*] The estimated values are mean ± SD from three independent experiments

[**] Total volume distribution for 2TCM estimation: $V_T = K_1/k_2 *(1+k_3/k_4)$;

[***] Total volume distribution for Logan plot estimation: V_T = slope of the Logan plot.

Table 2

Kinetics[*] and occupancy of (−)-[11C]TZ659 following pharmacological pretreatment

Drugs and doses (mg/kg)	Kinetic parameters for striatal uptake					
	LoganREF		SRTM			
	BP_{ND}	Occ%	BP_{ND}	R_1	k_2 (min^{-1})	Occ %
Control[**]	1.5 ± 0.26	0	1.5 ± 0.12	0.75 ± 0.09	0.055 ± 0.034	0
(−)-Vesamicol—0.25	0.43	72	0.39	0.87	0.049	75
(−)-Vesamicol—0.125	0.33	78	0.36	0.82	0.035	77
(−)-Vesamicol—0.05	0.68	56	0.61	0.83	0.028	60
(−)-Vesamicol—0.01	0.69	55	0.85	0.85	0.033	44
(+)-Pentazocine—1.0	1.2	N/A	1.6	0.86	0.029	N/A
***S*-(−)-Eticlopride—0.025**	2.6	N/A	2.7	1.1	0.053	N/A

[*]
Reference region (cerebellar hemisphere) based modeling.

[**]
Averaged from all six baseline scans including four from Subject A and two from Subject B.

N/A: Not applicable